RESEARCH ARTICLE

Impact of Joule Heating and Viscous Dissipation on MHD Slip Flow of Tangent Hyperbolic Aluminum Alloys (AA7072-AA7075/H_2O) in a Porous Medium with Activation Energy

Waqas Ahmad [1,*]

[1] Department of Physical and Numerical Sciences, Qurtuba University of Science and Information Technology, Peshawar 25100, Pakistan

Abstract

This study investigates the two-dimensional magnetohydrodynamic (MHD) slip flow of a tangent-hyperbolic (TGH) aluminum-alloy hybrid nanofluid over a stretching surface in a porous medium. The model incorporates magnetic effects, velocity and thermal slip, thermal radiation, heat generation, viscous dissipation, chemical reaction, and activation energy. The governing nonlinear partial differential equations are transformed into ordinary differential equations using similarity transformations and solved numerically in MATLAB using the `bvp4c` solver. The effects of key parameters on the velocity, temperature, and concentration profiles are analyzed, together with the skin-friction coefficient, Nusselt number, and Sherwood number. The results show that velocity decreases with increasing velocity-slip, porous-medium, and magnetic parameters, but increases with the fluid-thickness parameter. Temperature increases with nanoparticle volume fraction, magnetic parameter, Eckert number, velocity-slip parameter, and porous-medium parameter, whereas thermal radiation and the thermophoresis parameter reduce temperature. Concentration decreases with increasing activation energy, chemical-reaction parameter, velocity-slip parameter, and Schmidt number, but increases with the Lewis number. Comparison with previously published limiting-case results demonstrates good agreement and validates the numerical solution. These findings highlight the importance of controlling physical parameters in regulating momentum, heat, and mass transfer in MHD hybrid nanofluids, with potential applications in heat exchangers, enhanced oil recovery, environmental remediation, thermal management, and materials processing.

Keywords: Tangent hyperbolic hybrid nanofluid, Joule heating, Slip flow, Viscous dissipation, Thermal radiation, Activation energy, Porous medium.

Submitted: 03 June 2026
Revised: 09 August 2026
Accepted: 11 August 2026
Published: 05 September 2026

Vol. 2, **No.** 4, 2026.
10.62762/JAM.2026.103707

***Corresponding author:**
✉ Waqas Ahmad
waqas64065@gmail.com

Citation
Ahmad, W. (2026). Impact of Joule Heating and Viscous Dissipation on MHD Slip Flow of Tangent Hyperbolic Aluminum Alloys (AA7072-AA7075/H_2O) in a Porous Medium with Activation Energy. *ICCK Journal of Applied Mathematics*, 2(4), 251–265.

Nomenclature

Symbols

We	Weissenberg parameter
K	Porous-medium parameter
D_B	Brownian motion coefficient
β	Thermal slip parameter
D_T	Thermophoretic diffusion coefficient
C_{fx}	Skin-friction coefficient
δ	Temperature difference parameter
Kr	Chemical reaction parameter
E	Activation energy
C_p	Specific heat $(\mathrm{J\,kg^{-1}\,K^{-1}})$
σ^*	Stefan–Boltzmann constant
M	Magnetic parameter
n	Fluid-thickness (power-law) parameter
Nu_x	Nusselt number
Pr	Prandtl number
q_r	Thermal radiation heat flux $(\mathrm{W\,m^{-2}})$
Ec	Eckert number
Le	Lewis number
Rd	Thermal radiation parameter
Re	Reynolds number
Q	Heat generation/absorption parameter
γ	Velocity slip parameter
Re_x	Local Reynolds number
h	Heat-transfer coefficient
T_w	Surface temperature (K)
T	Fluid temperature (K)
T_∞	Free-stream temperature (K)
x, y	Cartesian coordinates (m)
u, v	Fluid velocity components $(\mathrm{m\,s^{-1}})$

Greek letters

κ	Thermal conductivity
ϕ	Nanoparticle volume fraction
μ	Viscosity
η	Similarity variable
(ρC_p)	Heat capacity
ρ	Fluid density
Φ	Dimensionless concentration
θ	Dimensionless temperature

Subscripts

0	Reference condition
f	Base fluid
w	Wall
∞	Free stream $(y \to \infty)$
hnf	Hybrid nanofluid

Abbreviations

Abbreviation	Description
NNFs	Non-Newtonian fluids
PDEs	Partial differential equations
NF	Nanofluid
THNF	Ternary hybrid nanofluid
ODEs	Ordinary differential equations
TBL	Thermal boundary layer
MHD	Magnetohydrodynamic
AE	Activation energy
NP	Nanoparticles
BL	Boundary layer
TGH	Tangent hyperbolic
HNF	Hybrid nanofluid
MBL	Momentum boundary layer
TC	Thermal conductivity
2D	Two-dimensional
LNN	Local Nusselt number
TGHNF	Tangent-hyperbolic hybrid nanofluid

1 Introduction

Non-Newtonian fluids (NNFs) are extensively employed in industrial and technical settings. The components of these fluids interact in complicated ways, exhibiting nonlinear energy-transport behaviour and a nonlinear stress–strain relationship. The tangent hyperbolic (TGH) fluid is an important non-Newtonian model that effectively characterises shear-thinning behaviour. Tangent-hyperbolic fluids include paint, blood, cream cheese, sauce, and magma. This model offers benefits including flexibility, computational simplicity, and physical stability compared with other models, and it is based on realistic principles of liquids rather than an imagined relationship. It accurately predicts shear-thinning behaviour and gives a realistic representation of blood flow. The thickness of the momentum boundary layer (MBL) is significantly influenced by the porous medium; consequently, numerous researchers have investigated TGH fluids and hybrid nanofluids in relation to fluid-flow and heat-transfer problems.

Senthilvadivu *et al.* [1] performed a numerical analysis of blood-based magnetohydrodynamic TGH hybrid-nanofluid flow through a permeable stretched surface with variable thermal conductivity (TC) and cross-diffusion. Amjad *et al.* [2] presented a computational investigation of MHD TGH nanofluid flow over an exponentially stretching surface; both the magnetic parameter and Weissenberg number reduce the boundary layer (BL). Jawad *et al.* [3] investigated thermal radiative tangent hyperbolic nanofluid flow over a bidirectional stretching surface with Joule heating and chemical reaction effects. Alqahtani *et al.* [4] numerically studied forced-convective TGH nanofluid motion across a permeable wedge under heat generation and the Lorentz force; the permeability component decreases the fluid flow.

Siddique *et al.* [5] analyzed the dynamics of a ternary hybrid nanofluid (THNF) over a non-linear stretching surface with motile microorganisms under concentration-dependent viscosity. Moltot *et al.* [6] analyzed unsteady MHD flow of a tangent hyperbolic ternary hybrid nanofluid through a Darcy–Forchheimer porous medium over a permeable stretching sheet with variable thermal conductivity. Choudhary *et al.* [7] investigated MHD thermal and solutal stratified stagnation flow of TGH fluid induced by a stretching cylinder with dual convection. Moatimid *et al.* [8] examined TGH micropolar nanofluid flow over an extending layer in a permeable surface. Alhefthi *et al.* [9] investigated convective BL flow of MHD TGH nanofluid over a stratified sheet with chemical reaction. Ahmed *et al.* [10] numerically investigated MHD flow of hyperbolic tangent nanofluid over a nonlinear stretching sheet, examining velocity, temperature, and concentration profiles under various physical parameters. Das and Majumdar [11] examined bioconvective MHD TGH nanofluid flow over a stretching surface under convective-heat and slip conditions. Kumar *et al.* [12] numerically modelled nanoparticle size and thermal radiation with a magnetic-field effect for THNF. Nadeem *et al.* [13] conducted a numerical study of unsteady tangent hyperbolic fuzzy hybrid nanofluid flow over an exponentially stretching surface using fuzzy set theory to handle parameter uncertainty. Wu *et al.* [14] examined entropy generation in radiative TGH nanofluid motion with gyrotactic microorganisms and activation energy. Panda *et al.* [15] proposed a biomathematical model of gyrotactic microorganisms and bimolecular reactions on a bidirectional THNF with Nield boundary conditions. Some further recent studies on non-Newtonian fluids are [16–21].

The maximum energy required to initiate a chemical reaction is known as the activation energy (AE); it may be viewed as the energy needed to break bonds between reactant molecules. When the AE is higher, the reaction proceeds more slowly. Irfan *et al.* [22] investigated thermophoretic dispersion of nanoparticles in a nonlinear-radiative Maxwell nanofluid with activation energy. Shahzad *et al.* [23] analyzed MHD tangent hyperbolic nanofluid flow past a stretching sheet incorporating chemical reaction, viscous dissipation, and Joule heating effects. Qaiser *et al.* [24] examined AE and entropy optimization in radiative stagnation-point flow of nanofluids with viscous dissipation and cross-diffusion. Hussain *et al.* [25] incorporated AE and gyrotactic bacteria into the chemically reactive, bio-convective motion of micropolar nanoparticles. Asjad *et al.* [26] analyzed the impact of chemical reaction and bioconvection on MHD nanofluid flow over an exponentially stretching surface. Çolak [27] evaluated Arrhenius-AE and temperature-dependent-viscosity effects on Maxwell-nanofluid bio-convective flow with partial slip using an AI method. Ali *et al.* [28] studied concentration-associated transport with gyrotactic microorganisms and heat radiation with AE on an unsteady Riga surface. Khan *et al.* [29] investigated AE and binary chemical reactions in swirling flow. Irshad *et al.* [30] examined slip-enhanced MHD Williamson-nanofluid dynamics with thermal radiation and chemical reaction. Zeb *et al.* [31] investigated melting heat transfer and thermal radiation on MHD tangent hyperbolic nanofluid flow over a stretching surface with chemical reaction and activation energy. Ahmad *et al.* [32] examined Soret–Dufour effects for MHD mixed-convective Maxwell hybrid-nanofluid flow in a porous medium with AE. Irfan [33] studied Joule-heating energy transport with Arrhenius AE in a Maxwell nanofluid. Jameel *et al.* [34] analyzed entropy-driven optimization of nonlinear-radiative Sutterby-nanofluid flow with the Hall effect and AE. Rashid *et al.* [35] studied entropy generation in MHD blood flow of a hybrid nanofluid with nonlinear-radiative heat flux.

Alatawi *et al.* [36] studied the dynamic behaviour of Casson hybrid nanofluids under coupled boundary slip and reaction-diffusion processes on a stretching sheet. Alsenafi and Ferdows [37] examined the effects of chemical reaction and thermal slip on free-convective nanofluid flow from a horizontal plate in a porous medium. Prajapati and Meher [38] examined two-dimensional MHD tangent hyperbolic hybrid nanofluid flow over a porous stretched sheet under velocity and thermal slip conditions with different base fluids. Ahmad [39] studied 3D MHD rotating Casson hybrid-nanofluid flow under convective boundary conditions and velocity slip with Darcy–Forchheimer effects. Yusuf *et al.* [40] examined Thomson–Troian slip conditions for a hybrid nanofluid over a Riga plate. Revathi *et al.* [41] performed a multiple-linear-regression analysis of THNF flow with quadratic radiation and second-order slip. Bilal and Yasir [42] studied mass-transpiration effects on the heat-transfer efficiency of a THNF with velocity slip.

This paper investigates the MHD flow of a TGH aluminum-alloy hybrid nanofluid (AA7072–AA7075/H_2O) through a porous medium with slip effects over a linearly stretched surface. The shooting-based reduction is combined with the `bvp4c` collocation solver to resolve the governing equations numerically, and the results are presented in tables and graphs. The novelty of the present study lies in the investigation of the volume-fraction effects of AA7072–AA7075 hybrid nanoparticles dispersed in water under the combined influence of Joule heating, activation energy, and viscous dissipation. The velocity profile rises with the fluid-thickness parameter and falls with increasing slip, porous-medium, and magnetic-field parameters. Nanoparticle volume fraction, slip parameter, Eckert number, thermophoresis parameter, magnetic parameter, and porous-medium parameter all raise the temperature profile; however, the temperature diminishes as the radiation component increases. The concentration profile rises with the Lewis number, whereas a higher Schmidt number, chemical-reaction parameter, activation energy, and slip factor decrease it. In metallurgical and fusion-reactor applications, magnetic fields provide a means of controlling temperature and fluid flow.

The main objectives of the present investigation are:

1. How do the magnetic parameter, porous medium, and Weissenberg parameter influence the velocity distribution of the hybrid nanofluid?
2. How do Brownian motion and thermophoresis influence the temperature and concentration distributions?
3. What are the effects of the magnetic parameter, porous-medium parameter, Eckert number, radiation parameter, Schmidt number, Lewis number, activation energy, and slip parameters on the flow behaviour?
4. How do variations in the physical parameters affect key engineering quantities such as the skin-friction coefficient, local Nusselt number, and Sherwood number?

2 Problem Statement

Shear-thinning behaviour, typical of many industrial fluids, is accurately captured by the tangent-hyperbolic model. Using a porous medium to simulate flow through granular or fibrous substances makes the model more realistic. This work investigates the 2D incompressible flow of an aluminum-alloy nanomaterial over a stretched sheet. Porous-medium resistance, velocity slip, thermal radiation, Joule heating, heat generation/absorption, thermal slip, activation energy, and viscous-dissipation effects are all included; the concentration equation accounts for activation energy. The prototype simulation of the configuration is shown in Figure 1. The sheet stretches along the x-axis at the rate $u_w(x) = ax$, and the y-axis is orthogonal to the surface. The wall temperature follows $T_w(x)$ along the stretched layer, with ambient temperature T_∞ and ambient concentration C_∞. A single-phase nanofluid model is adopted: nanoparticles are assumed uniformly distributed in the base fluid and in thermal equilibrium with it (owing to the small particle size and rapid heat transfer), of uniform size, with negligible agglomeration and a stable, dilute dispersion.

Under these assumptions, the governing PDEs (continuity, momentum, energy, and concentration), consistent with earlier studies [43, 44], are

$$\frac{\partial u}{\partial x} + \frac{\partial v}{\partial y} = 0, \tag{1}$$

$$\begin{aligned} u\frac{\partial u}{\partial x} + v\frac{\partial u}{\partial y} &= \frac{\mu_{hnf}}{\rho_{hnf}}\left[(1-n) + \sqrt{2}\,n\Gamma\frac{\partial u}{\partial y}\right]\frac{\partial^2 u}{\partial y^2} \\ &\quad - \frac{\sigma_{hnf}}{\rho_{hnf}}B_0^2 u - \frac{\mu_{hnf}}{\rho_{hnf}}\frac{u}{k_p}, \end{aligned} \tag{2}$$

$$\begin{aligned} u\frac{\partial T}{\partial x} + v\frac{\partial T}{\partial y} &= \frac{k_{hnf}}{(\rho C_p)_{hnf}}\frac{\partial^2 T}{\partial y^2} + \frac{16\sigma^* T_\infty^3}{3k^*(\rho C_p)_{hnf}}\frac{\partial^2 T}{\partial y^2} \\ &+ \frac{(\rho C)_p}{(\rho C_p)_{hnf}}\left[D_B\frac{\partial C}{\partial y}\frac{\partial T}{\partial y} + \frac{D_T}{T_\infty}\left(\frac{\partial T}{\partial y}\right)^2\right] \\ &+ \frac{\sigma_{hnf}}{(\rho C_p)_{hnf}}B_0^2 u^2 + \frac{\mu_{hnf}}{(\rho C_p)_{hnf}}\left(\frac{\partial u}{\partial y}\right)^2 \\ &+ \frac{Q_0}{(\rho C_p)_{hnf}}(T - T_\infty), \end{aligned} \tag{3}$$

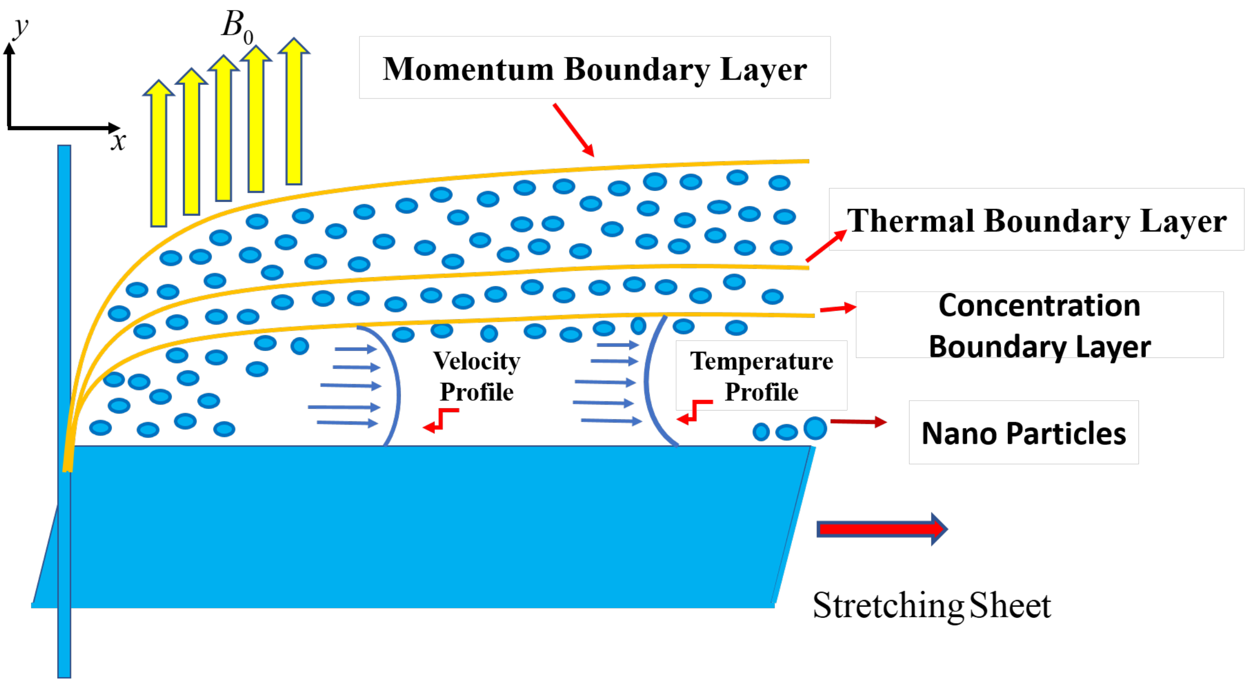

Figure 1. Flow configuration [32].

$$u\frac{\partial C}{\partial x}+v\frac{\partial C}{\partial y}=\frac{D_T}{T_\infty}\frac{\partial^2 T}{\partial y^2}+D_B\frac{\partial^2 C}{\partial y^2} - k_r^2(C-C_\infty)\left(\frac{T}{T_\infty}\right)^m \exp\left(-\frac{E}{kT}\right). \tag{4}$$

With the boundary conditions

$$u=u_w(x)+A\frac{\partial u}{\partial y},\ v=0,\ T=T_w(x)+B\frac{\partial T}{\partial y}, \quad C=C_w,\ \text{at } y=0, \quad C\to C_\infty,\ T\to T_\infty,\ u\to 0,\ \text{as } y\to\infty. \tag{5}$$

Here A is the velocity-slip coefficient and B the thermal-slip coefficient; the condition $v=0$ at $y=0$ indicates an impermeable surface. The velocity and temperature slips account for incomplete fluid–surface interaction, important in microscale and rarefied flows.

Employing the similarity transformation

$$u=axf'(\eta),\ v=-\sqrt{a\nu_f}\,f(\eta),\ \Psi=\sqrt{a\nu_f}\,xf(\eta), \quad \eta=\sqrt{\frac{a}{\nu_f}}\,y,\ \theta(\eta)=\frac{T-T_\infty}{T_w-T_\infty},\ \Phi(\eta)=\frac{C-C_\infty}{C_w-C_\infty}, \tag{6}$$

equation (1) is identically satisfied, and equations (2)–(5) reduce to

$$\left[(1-n)+nWe\,f''\right]\frac{\mu_{hnf}}{\mu_f}f'''+\frac{\rho_{hnf}}{\rho_f}(ff''-f'^2) - \frac{\mu_{hnf}}{\mu_f}Kf'-\frac{\sigma_{hnf}}{\sigma_f}Mf'=0, \tag{7}$$

$$\left[\frac{k_{hnf}/k_f}{(\rho C_p)_{hnf}/(\rho C_p)_f}+\frac{4R}{3\,(\rho C_p)_{hnf}/(\rho C_p)_f}\right]\theta'' + Pr\left\{f\theta'-2\theta f'+\frac{Q}{(\rho C_p)_{hnf}/(\rho C_p)_f}\theta\right\}+\frac{Nc}{Le}\theta'\Phi' + \frac{\mu_{hnf}/\mu_f}{(\rho C_p)_{hnf}/(\rho C_p)_f}Ec\,f''^2+\frac{Nc}{Le\,Nbt}\theta'^2 + \frac{\sigma_{hnf}/\sigma_f}{(\rho C_p)_{hnf}/(\rho C_p)_f}M\,Ec\,f'^2=0, \tag{8}$$

$$\Phi''+Sc\,f\Phi'-2Sc\,\Phi f'+\left(1+\frac{1}{Nbt}\right)\theta'' - Sc\,Kr\,(1+\delta\theta)^m\exp\left(-\frac{E}{1+\delta\theta}\right)\Phi(\eta)=0, \tag{9}$$

with boundary conditions

$$f'=1+\gamma f'',\ f=0,\ \theta=1+\beta\theta',\ \Phi=1,\ \text{at } \eta=0, \quad f'\to 0,\ \Phi\to 0,\ \theta\to 0,\ \text{as } \eta\to\infty. \tag{10}$$

The dimensionless variables are defined as: Weissenberg parameter We, porous-medium parameter K, magnetic parameter M, Prandtl number Pr, radiation parameter R, Eckert number Ec, temperature-difference parameter δ, chemical-reaction parameter Kr, dimensionless activation energy E, Schmidt number Sc, velocity-slip parameter γ, and thermal-slip parameter β.

2.1 Engineering Quantities

The skin-friction coefficient, local Nusselt number, and Sherwood number are

$$\begin{aligned} C_{fx}\sqrt{Re_x} &= \left[1+\tfrac{1}{2}We\, f''\right]\frac{\mu_{hnf}}{\mu_f} f''(0), \\ \frac{Nu_x}{\sqrt{Re_x}} &= -\frac{k_{hnf}}{k_f}\left(\theta'(0)+Rd\right), \\ \frac{Sh_x}{\sqrt{Re_x}} &= -\Phi'(0), \\ \text{where } Re_x &= \frac{x\,u_w(x)}{\nu_f}. \end{aligned} \tag{11}$$

3 Research Methodology

The system of ODEs (7)–(9), subject to constraints (10), is solved using `bvp4c`, a numerical method built into MATLAB, after reducing the equations to a first-order system as discussed in refs [45, 46]. `bvp4c` implements a three-stage Lobatto IIIa collocation formula with fourth-order accuracy and automatic mesh adaptation; it is robust and computationally efficient. For a unique, stable solution, the boundary-value problem must be well posed. The overall solution procedure is summarised in Figure 2.

The thermophysical properties of the hybrid nanofluid are [47]:

Heat capacity:

$$\begin{aligned}(\rho C_p)_{hnf} = &(1-\phi_{AA7072+AA7075})(\rho C_p)_{H_2O} \\ &+ \phi_{AA7072}(\rho C_p)_{AA7072} + \phi_{AA7075}(\rho C_p)_{AA7075}.\end{aligned}$$

Thermal conductivity:

$$\frac{k_{hnf}}{k_f} = \frac{\dfrac{\phi_{AA7072}k_{AA7072}+\phi_{AA7075}k_{AA7075}}{\phi_{AA7072+AA7075}} + 2k_{H_2O} + 2(\phi_{AA7072}k_{AA7072}+\phi_{AA7075}k_{AA7075}) - 2k_{H_2O}\phi_{AA7072+AA7075}}{\dfrac{\phi_{AA7072}k_{AA7072}+\phi_{AA7075}k_{AA7075}}{\phi_{AA7072+AA7075}} + 2k_{H_2O} + (\phi_{AA7072}k_{AA7072}+\phi_{AA7075}k_{AA7075}) - k_{H_2O}\phi_{AA7072+AA7075}}.$$

Density:

$$\begin{aligned}\rho_{hnf} &= \rho_{AA7072}\phi_{AA7072} + \rho_{AA7075}\phi_{AA7075} \\ &\quad + \rho_{H_2O}(1-\phi_{AA7072+AA7075}), \\ \phi_{hnf} &= \phi_{AA7072}+\phi_{AA7075}\end{aligned}$$

Dynamic viscosity:

$$\frac{\mu_{hnf}}{\mu_f} = (1-\phi_{AA7072+AA7075})^{-2.5}.$$

Electrical conductivity:

$$\frac{\sigma_{hnf}}{\sigma_f} = \frac{\dfrac{\phi_{AA7072}\sigma_{AA7072}+\phi_{AA7075}\sigma_{AA7075}}{\phi_{AA7072+AA7075}} + 2\sigma_{H_2O} + 2(\phi_{AA7072}\sigma_{AA7072}+\phi_{AA7075}\sigma_{AA7075}) - 2\sigma_{H_2O}\phi_{AA7072+AA7075}}{\dfrac{\phi_{AA7072}\sigma_{AA7072}+\phi_{AA7075}\sigma_{AA7075}}{\phi_{AA7072+AA7075}} + 2\sigma_{H_2O} + (\phi_{AA7072}\sigma_{AA7072}+\phi_{AA7075}\sigma_{AA7075}) - \sigma_{H_2O}\phi_{AA7072+AA7075}}.$$

Table 1. Base-fluid and hybrid-nanoparticle empirical estimations [48].

Property	AA7072	AA7075	H_2O
k ($\mathrm{W\,m^{-1}\,K^{-1}}$)	222	173	0.613
ρ ($\mathrm{kg\,m^{-3}}$)	2720	2810	997.1
C_p ($\mathrm{J\,kg^{-1}\,K^{-1}}$)	893	960	4179
σ ($\mathrm{S\,m^{-1}}$)	–	–	–
Pr	6.2		

To generate a first-order system, the new variables are introduced:

$$\begin{aligned} &f=\Lambda_1,\ f'=\Lambda_2,\ f''=\Lambda_3,\ f'''=\Lambda\Lambda_1, \\ &\theta=\Lambda_4,\ \theta'=\Lambda_5,\ \theta''=\Lambda\Lambda_2, \\ &\Phi=\Lambda_6,\ \Phi'=\Lambda_7,\ \Phi''=\Lambda\Lambda_3. \end{aligned} \tag{12}$$

The resulting first-order ODEs with their boundary conditions are

$$\begin{aligned}\Lambda\Lambda_1 = &\frac{A_2}{A_1\left[(1-n)+nWe\,\Lambda_3\right]}\left[\Lambda_2^2-\Lambda_1\Lambda_3+\frac{A_4}{A_2}M\Lambda_2\right. \\ &\left.+\frac{A_1}{A_2}K\Lambda_2\right],\end{aligned} \tag{13}$$

$$\begin{aligned}\Lambda\Lambda_2 = &\frac{1}{\left(\dfrac{A_3}{A_5}+\dfrac{4Rd}{3A_5}\right)}\left[-Pr(\Lambda_1\Lambda_5-2\Lambda_2\Lambda_4)-\frac{Pr}{A_5}Q\Lambda_4\right. \\ &\left.-\frac{Nc}{Le}\Lambda_5\Lambda_7-\frac{Nc}{Ntb\,Le}\Lambda_5^2-\frac{A_4}{A_5}M\,Ec\,\Lambda_2^2-\frac{A_1}{A_5}Ec\,\Lambda_3^2\right],\end{aligned} \tag{14}$$

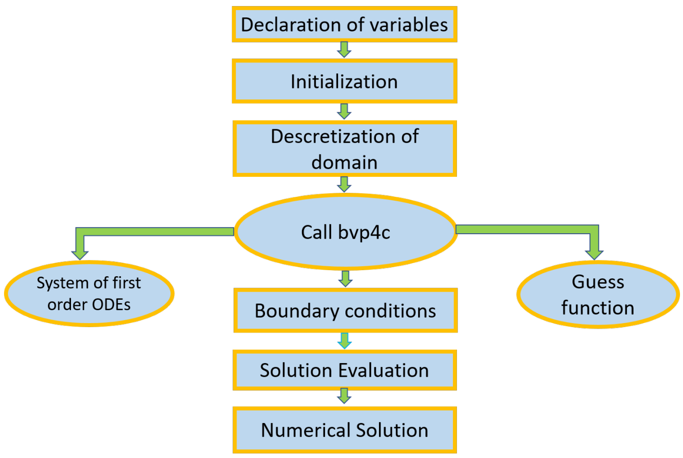

Figure 2. Solution methodology. Reproduced from [21].

$$\Lambda\Lambda_3 = -Sc\,\Lambda_1\Lambda_7 + 2Sc\,\Lambda_6\Lambda_2 + \left(1+\frac{1}{Nbt}\right)\Lambda\Lambda_2 + Sc\,Kr\,(1+\delta\Lambda_4)^m \exp\left(-\frac{E}{1+\delta\Lambda_4}\right)\Lambda_6, \quad (15)$$

along with

$$\Lambda_2(0) - 1 - \gamma\Lambda_3(0),\ \Lambda_1(0),\ \Lambda_4(0) - 1 - \beta\Lambda_5(0),\ \Lambda_6(0) - 1,\ \Lambda_2(\infty),\ \Lambda_4(\infty),\ \Lambda_6(\infty). \quad (16)$$

For all computations, a step length of 0.01 and a convergence criterion of 10^{-6} are used, and the domain $[0,\infty)$ is truncated to $[0,3]$ while satisfying the far-field conditions.

4 Results and Discussion

This study analyzes the effects of Joule heating and thermal radiation on MHD slip flow of a tangent-hyperbolic ($AA7072$–$AA7075/H_2O$) hybrid nanofluid in a porous medium with activation energy. This section illustrates how different physical parameters affect the temperature θ, velocity f', and concentration Φ profiles. The numerical solution of (13)–(15) is obtained by the `bvp4c` method. Table 1 lists the base-fluid and hybrid-nanoparticle empirical estimations. Table 2 compares $-\theta'(0)$ for limiting cases with previous studies. Tables 3 and 4 report the numerical values of the skin-friction coefficient, Nusselt number, and Sherwood number.

The magnetic parameter affects the velocity and temperature (Figures 3 and 4). The velocity decreases as M increases, because the Lorentz force opposes fluid motion and thins the momentum BL; the temperature rises because the magnetic field increases internal friction and heat generation, thickening

Table 2. Comparison of $-\theta'(0)$ at various Prandtl numbers.

Pr	Amer *et al.* [43]	Sheri *et al.* [44]	Present study
0.72	0.808631	0.810323	0.810327
1	1	1	1
3	1.923682	1.923679	1.923685
10	3.720673	3.720669	3.720677

Table 3. Numerical values of the skin-friction coefficient $-C_{fx}\sqrt{Re_x}$ and Nusselt number $Nu_x/\sqrt{Re_x}$ for various parameters. Dashes (–) in the $-C_{fx}\sqrt{Re_x}$ column for β indicate that the thermal-slip parameter does not enter the momentum equation and hence leaves the skin-friction coefficient unchanged from the baseline value. The repeated value for K reflects insensitivity of the skin-friction coefficient to the porous-medium parameter under the present baseline conditions ($M=0.5$, $n=0.5$, $We=0.5$, $\gamma=0.2$, $\beta=0.1$, $\phi=0.1$).

n	We	M	K	γ	β	ϕ	$-C_{fx}\sqrt{Re_x}$	$Nu_x/\sqrt{Re_x}$
0.5	0.5	0.2	0.5	0.2	0.1	0.1	−1.018574	0.882807
0.6	–	–	–	–	–	–	−1.039232	0.875942
0.7	–	–	–	–	–	–	−1.059211	0.869214
0.8	–	–	–	–	–	–	−1.078557	0.862616
–	0.6	–	–	–	–	–	−1.039051	0.878515
–	0.7	–	–	–	–	–	−1.058862	0.874306
–	0.8	–	–	–	–	–	−1.078050	0.870175
–	–	0.3	–	–	–	–	−0.911425	0.861548
–	–	0.4	–	–	–	–	−0.826075	0.841651
–	–	0.5	–	–	–	–	−0.756261	0.823031
–	–	–	0.6	–	–	–	−0.756261	0.770779
–	–	–	0.7	–	–	–	−0.756261	0.723476
–	–	–	0.8	–	–	–	−0.756261	0.680621
–	–	–	–	0.25	–	–	−1.017123	0.883079
–	–	–	–	0.30	–	–	−1.015671	0.883350
–	–	–	–	0.35	–	–	−1.014217	0.883622
–	–	–	–	–	0.2	–	−1.018574	0.827677
–	–	–	–	–	0.3	–	−1.018574	0.771211
–	–	–	–	–	0.4	–	−1.018574	0.713359
–	–	–	–	–	–	0.2	−0.967289	0.893173
–	–	–	–	–	–	0.3	−0.911194	0.904125
–	–	–	–	–	–	0.4	−0.849181	0.915769

the thermal BL (TBL). For the slip parameter (Figures 5–7), the velocity decreases with increasing slip (less momentum transferred from the sheet), the temperature rises (fluid particles remain longer in the heated region), and the concentration falls (less species transport from the surface).

Increasing the fluid-thickness parameter n enhances the velocity profile, as shown in Figure 8, because the effective resistance of the fluid decreases and momentum transfer from the stretching surface is strengthened. The effects of the porous-medium parameter K on the velocity and temperature profiles

Table 4. Numerical values of the Nusselt number $Nu_x/\sqrt{Re_x}$ and Sherwood number $Sh_x/\sqrt{Re_x}$ for various parameters.

n	We	M	Sc	Kr	E	Le	$Nu_x/\sqrt{Re_x}$	$Sh_x/\sqrt{Re_x}$
0.5	0.5	0.2	0.5	0.5	0.1	0.3	0.930614	4.82156336
0.6	–	–	–	–	–	–	0.923063	4.77581930
0.7	–	–	–	–	–	–	0.915715	4.73105714
0.8	–	–	–	–	–	–	0.908556	4.68722830
–	0.6	–	–	–	–	–	0.882159	4.50969940
–	0.7	–	–	–	–	–	0.832750	4.19183472
–	0.8	–	–	–	–	–	0.782360	3.86779069
–	–	0.3	–	–	–	–	0.842091	4.24414658
–	–	0.4	–	–	–	–	0.775159	3.82599413
–	–	0.5	–	–	–	–	0.723050	3.51190581
–	–	–	0.6	–	–	–	0.932348	4.80504112
–	–	–	0.7	–	–	–	0.933945	4.79106194
–	–	–	0.8	–	–	–	0.935417	4.77936109
–	–	–	–	0.6	–	–	0.933025	4.78456856
–	–	–	–	0.7	–	–	0.935142	4.75270406
–	–	–	–	0.8	–	–	0.937019	4.72499926
–	–	–	–	–	0.2	–	0.930651	4.82169949
–	–	–	–	–	0.3	–	0.930687	4.82183796
–	–	–	–	–	0.4	–	0.930724	4.82197873
–	–	–	–	–	–	0.4	0.984710	5.18642796
–	–	–	–	–	–	0.5	1.020136	5.42957786
–	–	–	–	–	–	0.6	1.044756	5.60030748

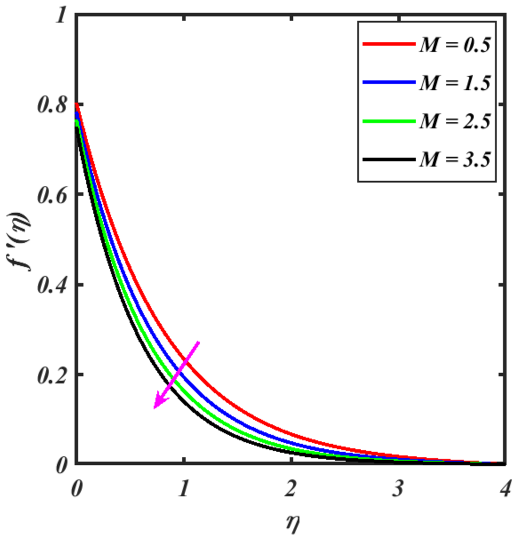

Figure 3. Impact of M on $f'(\eta)$.

are illustrated in Figures 9 and 10, respectively. As K increases, the velocity decreases because of the enhanced resistance offered by the porous medium, whereas the temperature increases owing to the reduced fluid motion and prolonged thermal interaction.

The influence of the thermal-slip parameter β on the temperature and concentration profiles is presented in Figures 11 and 12, respectively. Increasing β

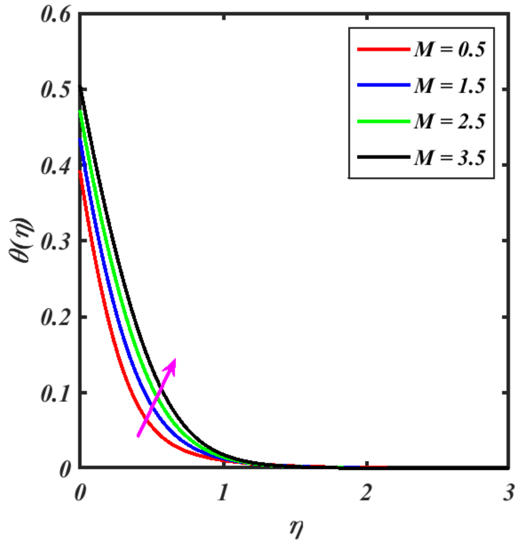

Figure 4. Impact of M on $\theta(\eta)$.

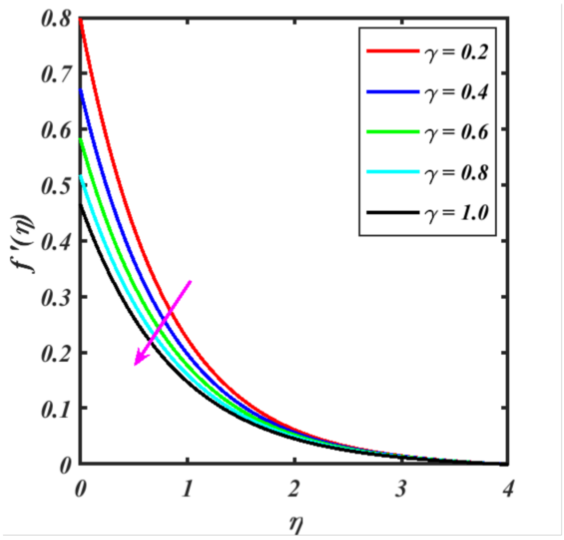

Figure 5. Impact of γ on $f'(\eta)$.

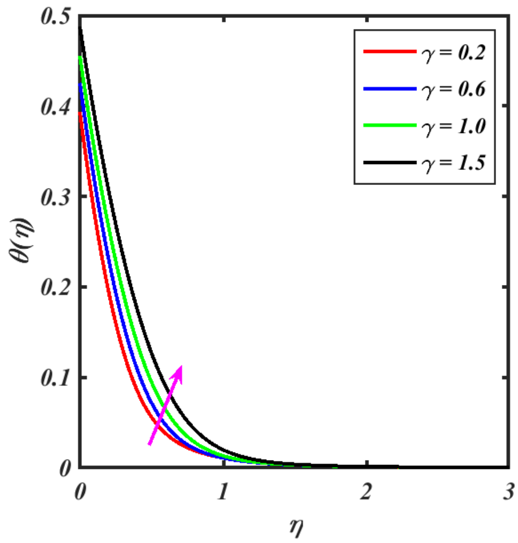

Figure 6. Impact of γ on $\theta(\eta)$.

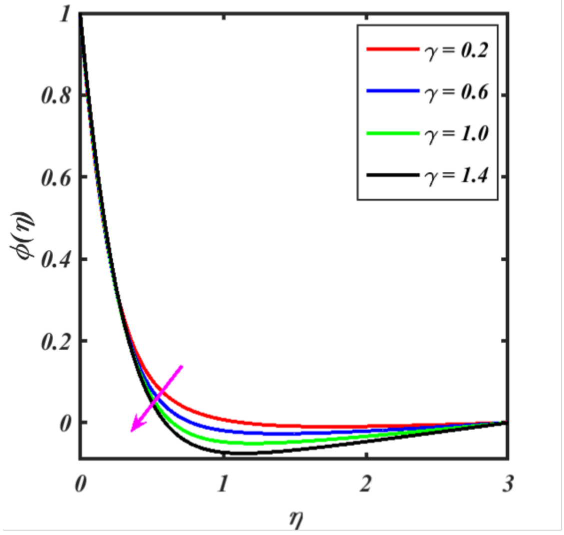

Figure 7. Impact of γ on $\Phi(\eta)$.

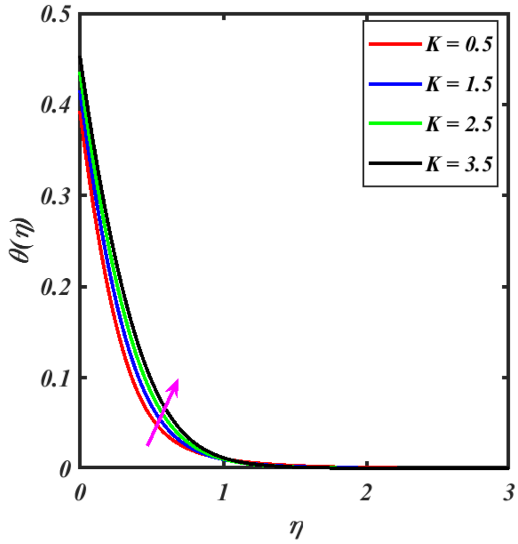

Figure 10. Impact of K on $\theta(\eta)$.

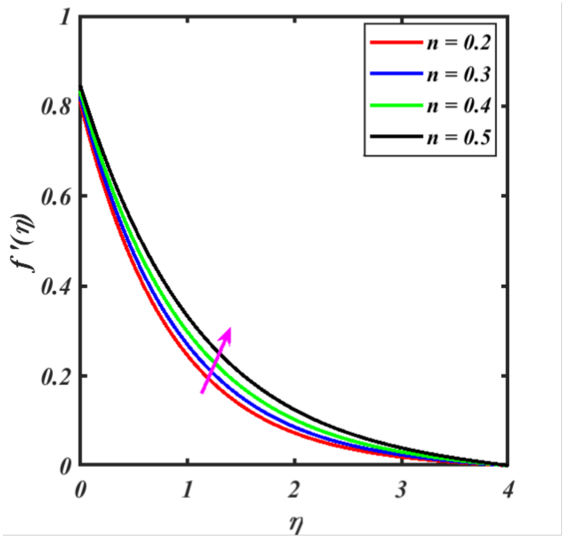

Figure 8. Impact of n on $f'(\eta)$.

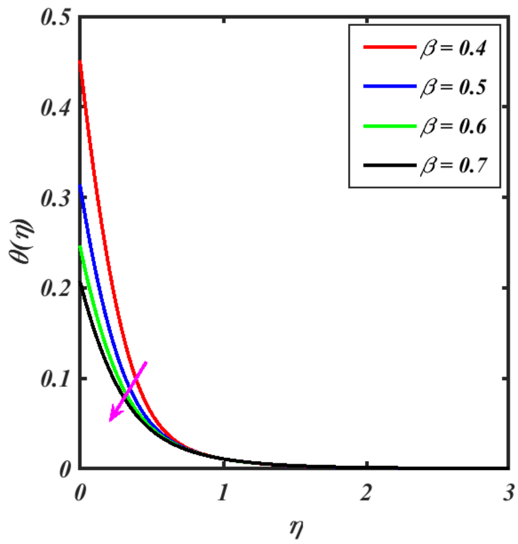

Figure 11. Impact of β on $\theta(\eta)$.

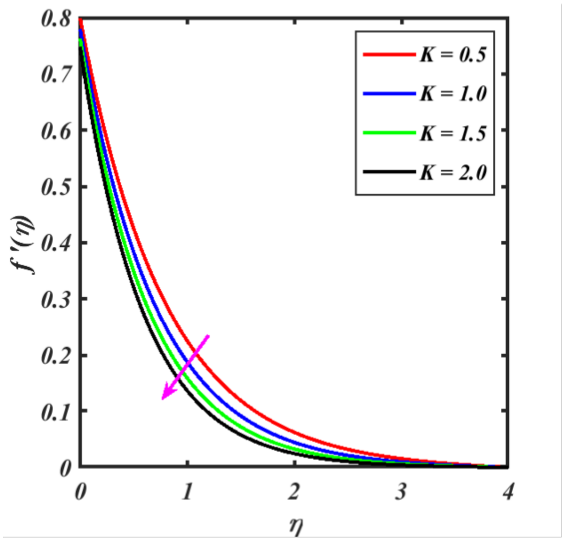

Figure 9. Impact of K on $f'(\eta)$.

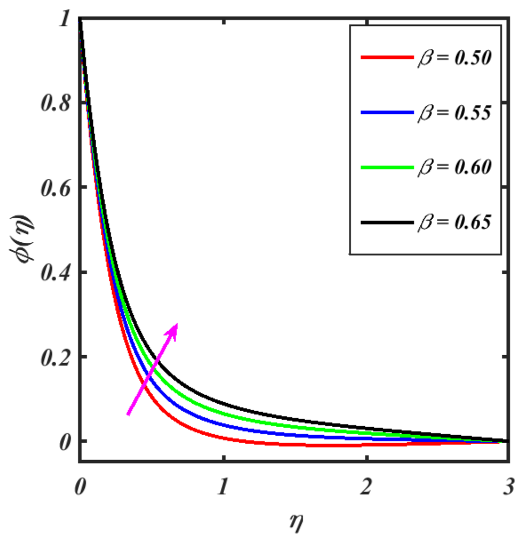

Figure 12. Impact of β on $\Phi(\eta)$.

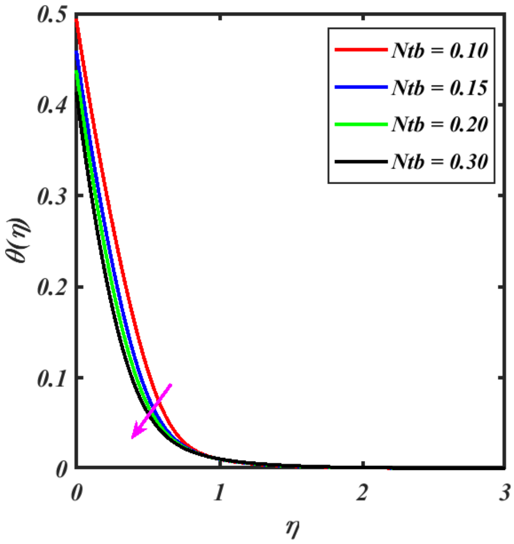

Figure 13. Impact of Nt on $\theta(\eta)$.

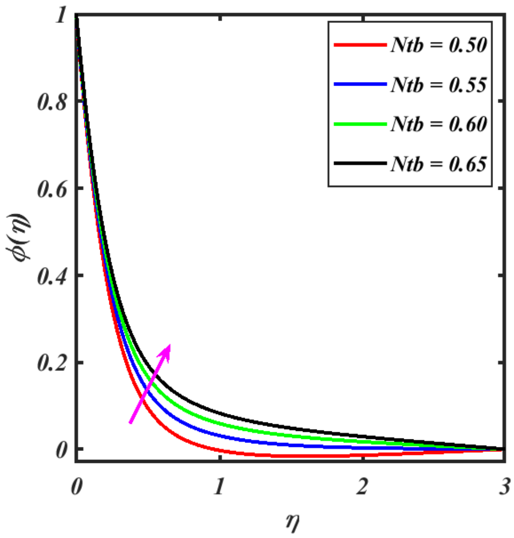

Figure 14. Impact of Nt on $\Phi(\eta)$.

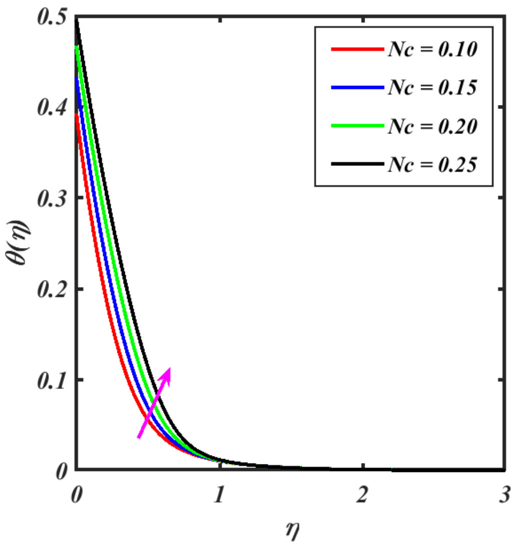

Figure 15. Impact of Nc on $\theta(\eta)$.

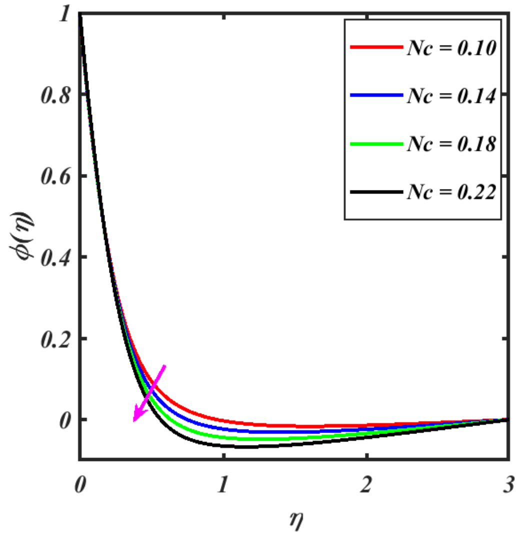

Figure 16. Impact of Nc on $\Phi(\eta)$.

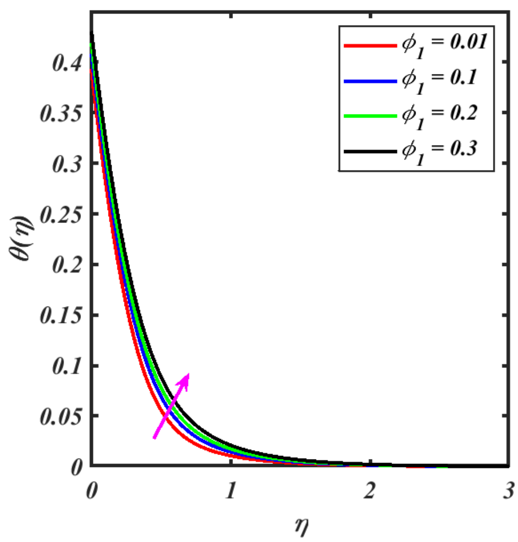

Figure 17. Impact of ϕ on $\theta(\eta)$.

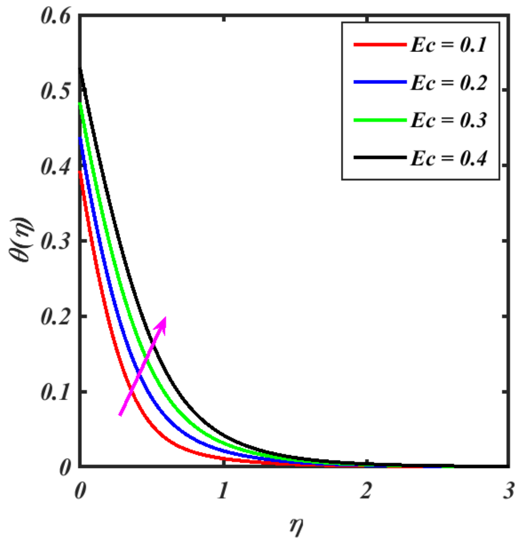

Figure 18. Impact of Ec on $\theta(\eta)$.

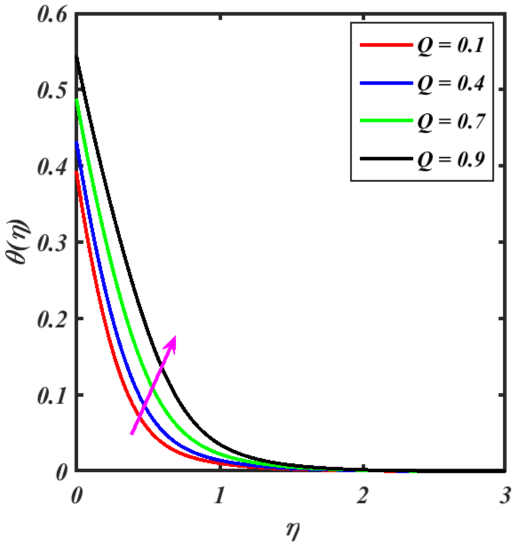

Figure 19. Impact of Q on $\theta(\eta)$.

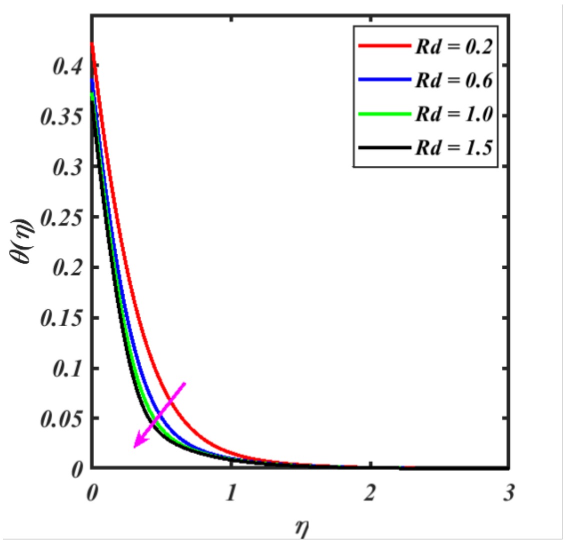

Figure 20. Impact of Rd on $\theta(\eta)$.

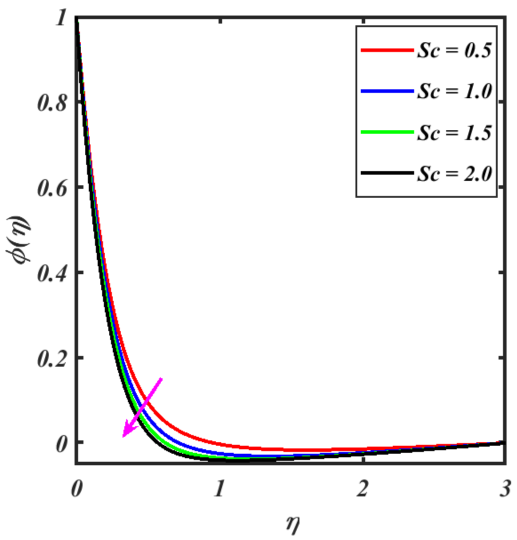

Figure 21. Impact of Sc on $\Phi(\eta)$.

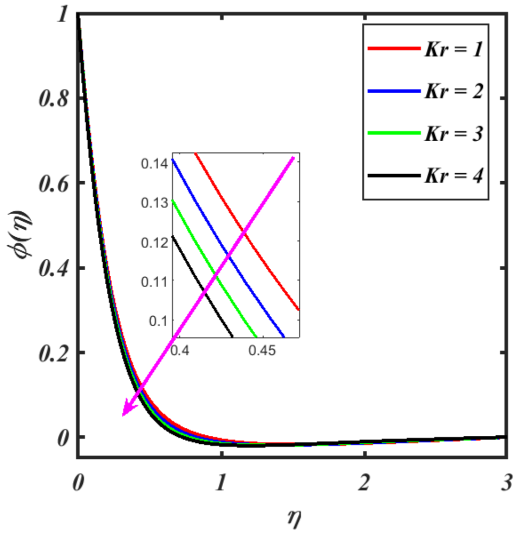

Figure 22. Impact of Kr on $\Phi(\eta)$.

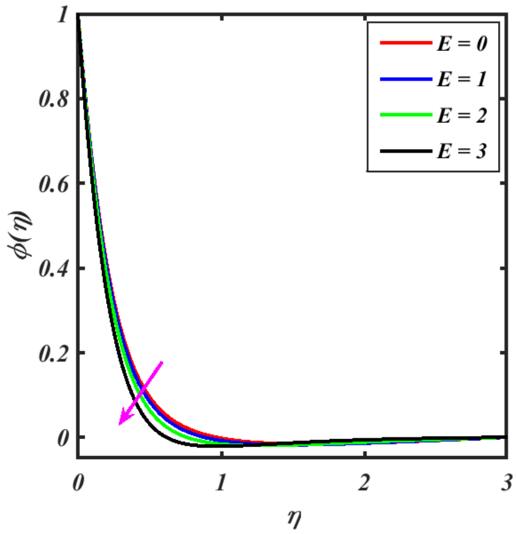

Figure 23. Impact of E on $\Phi(\eta)$.

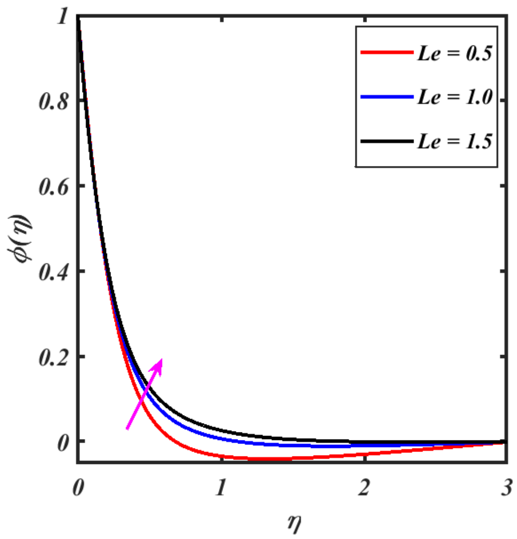

Figure 24. Impact of Le on $\Phi(\eta)$.

decreases the temperature profile because thermal slip reduces heat transfer from the stretching surface to the fluid, whereas the concentration profile increases. The effects of the thermophoresis parameter Nt on the temperature and concentration distributions are shown in Figures 13 and 14, respectively. An increase in Nt raises the temperature profile while also increasing the concentration profile. Figures 15 and 16 demonstrate the effects of the heat-capacity ratio Nc on the temperature and concentration profiles, respectively. Increasing Nc enhances the temperature profile but reduces the concentration profile.

Figure 17 illustrates the effect of the nanoparticle volume fraction ϕ on the temperature distribution. Increasing ϕ raises the temperature profile by modifying the effective thermophysical properties of the hybrid nanofluid. The influence of the Eckert number Ec is shown in Figure 18; a larger Ec increases the temperature because viscous dissipation converts kinetic energy into thermal energy. As illustrated in Figure 19, increasing the heat-generation parameter Q enhances the temperature profile owing to additional internal heat generation. In contrast, Figure 20 shows that increasing the radiation parameter Rd reduces the temperature profile under the present parameter settings.

The effects of the Schmidt number Sc, chemical-reaction parameter Kr, activation energy E, and Lewis number Le on the concentration profile are presented in Figures 21–24, respectively. As shown in Figure 21, the concentration decreases with increasing Sc because higher values of Sc correspond to weaker mass diffusivity. Figure 22 shows that increasing Kr decreases the concentration profile because of enhanced species consumption. The effect of activation energy E is depicted in Figure 23, where the concentration profile decreases with increasing E under the considered conditions. Finally, Figure 24 demonstrates that increasing the Lewis number Le enhances the concentration profile.

5 Conclusion

In this study, the velocity, temperature, and concentration distributions of an aluminum-alloy ($AA7072–AA7075/H_2O$) hybrid-nanofluid flow are investigated in relation to the porous medium, slip effects, thermal radiation, magnetic field, chemical reaction, and nanoparticle characteristics. The governing nonlinear ODEs are solved numerically to investigate the heat- and mass-transfer processes. The main conclusions are:

- The velocity profile decreases as the slip, magnetic, and porous-medium parameters increase, owing to resistive forces and reduced momentum transfer.
- The temperature decreases with the slip, thermal-slip, and radiation parameters but increases with the magnetic parameter, porosity parameter, Eckert number, and nanoparticle volume fraction.
- The concentration rises with the thermal-slip parameter and falls with the velocity-slip factor, nanoparticle volume fraction, Schmidt number, chemical-reaction parameter, and heat-capacity ratio.
- The concentration increases with the Lewis number and the thermophoresis parameter, owing to enhanced particle transport and reduced mass diffusion.
- The combination of a magnetic field and a porous medium significantly alters heat- and momentum-transfer characteristics.
- The Nusselt number and skin-friction coefficient are computed numerically.

This research has engineering applications in cooling systems and heat exchangers, enhanced oil recovery in porous reservoirs, nanofluid drug-delivery systems, thermal management of electronic equipment, and materials-processing industries.

5.1 Limitations of the Study

This study is based on a single-phase Buongiorno nanofluid model in which nanoparticle transport is described by Brownian motion and thermophoresis; interfacial interactions, sedimentation, and aggregation are neglected. Thermophysical properties are assumed constant, and thermal equilibrium between base fluid and nanoparticles is assumed. The analysis is restricted to steady, two-dimensional flow, and the results are numerical, without experimental confirmation.

5.2 Future Suggestions

Future work may adopt advanced multiphase nanofluid models that capture particle–fluid interactions, aggregation, sedimentation, and variable thermophysical properties; provide experimental validation; consider more complex geometries and unsteady flows; examine non-uniform magnetic fields for hybrid and ternary nanofluids; and apply optimization and machine-learning techniques for prediction of flow and heat-transfer characteristics.

Data Availability Statement

Data will be made available on request.

Funding

This work was supported without any funding.

Conflicts of Interest

The author declares no conflict of interest.

AI Use Statement

The author declares that no generative AI was used in the preparation of this manuscript.

Ethical Approval and Consent to Participate

Not applicable.

References

[1] Senthilvadivu, K., Loganathan, K., Abbas, M., & Alqahtani, M. S. (2024). Numerical study of blood-based MHD tangent hyperbolic hybrid nanofluid flow over a permeable stretching sheet with variable thermal conductivity and cross-diffusion. *Open Physics, 22*(1), 20240018. [CrossRef]

[2] Amjad, M., Khan, M. N., Ahmed, K., Ahmed, I., Akbar, T., & Eldin, S. M. (2023). Magnetohydrodynamics tangent hyperbolic nanofluid flow over an exponentially stretching sheet: Numerical investigation. *Case Studies in Thermal Engineering, 45*, 102900. [CrossRef]

[3] Jawad, M., Alam, M., & Nisar, K. S. (2023). Investigation of thermal radiative tangent hyperbolic nanofluid flow due to stretched sheet. *East European Journal of Physics*, (3), 233-239.[CrossRef]

[4] Alqahtani, A. M., Bilal, M., Riaz, M. B., Chammam, W., Shafi, J., Rahman, M. U., & Adnan. (2024). Forced convective tangent hyperbolic nanofluid flow subject to heat source/sink and Lorentz force over a permeable wedge: Numerical exploration. *Nanotechnology Reviews, 13*(1), 20240014. [CrossRef]

[5] Siddique, I., Abdal, S., Din, I. S. U., Awrejcewicz, J., Pawłowski, W., & Hussain, S. (2022). Significance of concentration-dependent viscosity on the dynamics of tangent hyperbolic nanofluid subject to motile microorganisms over a non-linear stretching surface. *Scientific Reports, 12*(1), 12765. [CrossRef]

[6] Moltot, A. T., Gorfie, E. H., Zergaw, G. A., & Dessie, H. (2025). Unsteady MHD flow of tangent hyperbolic ternary hybrid nanofluid in a darcy-forchheimer porous medium over a permeable stretching sheet with variable thermal conductivity. *F1000Research, 14*, 152.[CrossRef]

[7] Choudhary, S., Choudhary, P., Alessa, N., & Loganathan, K. (2023). MHD thermal and solutal stratified stagnation flow of tangent hyperbolic fluid induced by stretching cylinder with dual convection. *Mathematics, 11*(9), 2182. [CrossRef]

[8] Moatimid, G. M., Mohamed, M. A., Gaber, A. A., & Mostafa, D. M. (2023). Numerical analysis for tangent-hyperbolic micropolar nanofluid flow over an extending layer through a permeable medium. *Scientific Reports, 13*(1), 13522. [CrossRef]

[9] Alhefthi, R. K., Shahzadi, I., Khan, H. A., & Khan, N. (2024). Convective boundary layer flow of MHD tangent hyperbolic nanofluid over stratified sheet with chemical reaction. *AIMS Mathematics, 9*(7), 16901-16923. [CrossRef]

[10] Ahmed, I., Alghamdi, M., Amjad, M., Aziz, F., Akbar, T., & Muhammad, T. (2023). Numerical investigation of MHD flow of hyperbolic tangent nanofluid over a non-linear stretching sheet. *Heliyon, 9*(7). [CrossRef]

[11] Das, U. J., & Majumdar, N. M. (2025). Bio-convective magnetohydrodynamic flow of tangent hyperbolic nanofluid over a stretching surface with convective heat and slip conditions. *Journal of Heat and Mass Transfer Research, 12*(1), 91-102. [CrossRef]

[12] Kumar, P., Poonia, H., Ali, L., & Areekara, S. (2022). The numerical simulation of nanoparticle size and thermal radiation with the magnetic field effect based on tangent hyperbolic nanofluid flow. *Case Studies in Thermal Engineering, 37*, 102247. [CrossRef]

[13] Nadeem, M., Siddique, I., Riaz, Z., Makhdoum, B. M., Zulqarnain, R. M., & Sallah, M. (2023). Numerical study of unsteady tangent hyperbolic fuzzy hybrid nanofluid over an exponentially stretching surface. *Scientific Reports, 13*(1), 15551. [CrossRef]

[14] Wu, Y., Chaudhry, M., Maqbool, N., Tahir, M., Basit, M. A., & Imran, M. (2024). Entropy generation in radiative motion of tangent hyperbolic nanofluid in the presence of gyrotactic microorganisms and activation energy. *Frontiers in Physics, 12*, 1409318. [CrossRef]

[15] Panda, S., Nayak, B., Baithalu, R., & Mishra, S. R. (2024). Synergistic influence of gyrotactic microorganisms and bimolecular reaction on bidirectional tangent hyperbolic fluid with Nield boundary conditions: a biomathematical model. *Partial Differential Equations in Applied Mathematics, 12*, 100994. [CrossRef]

[16] Ahemd, M. F., Ali, F., Sidi, M. O., Zafar, S. S., & Saeed, A. M. (2026). The Darcy–Forchheimer tangent hyperbolic bioconvection flow of a nanofluid caused by a convective sheet: numerical study of the stagnation point. *Pramana, 100*(2), 43. [CrossRef]

[17] Riaz, A., DilNawaz, M., Akram, S., & Khan, S.

U. (2026). Effects of multiple slips on tangent hyperbolic-nanofluid with peristaltic flow having gyrotactic microorganisms under electromagnetic fields: a numerical approach. *International Journal of Ambient Energy, 47*(1), 2660197. [CrossRef]

[18] Lakshmi, R., Gireesha, B. J., & Venkatesh, P. (2026). Numerical evaluation of thermal and diffusive processes in magnetically induced tangent hyperbolic fluid flow with Dufour and Soret effects in a rotating channel. *Proceedings of the Institution of Mechanical Engineers, Part C: Journal of Mechanical Engineering Science, 240*(1), 264-284. [CrossRef]

[19] Irfan, M., Khan, M., Muhammad, T., Waqas, M., & Khan, W. A. (2022). Analysis of energy transport considering Arrhenius activation energy and chemical reaction in radiative Maxwell nanofluid flow. *Chemical Physics Letters, 793*, 139323. [CrossRef]

[20] Hamad, N. H. (2023). Numerical investigation of MHD tangent hyperbolic nanofluid flow across a vertical stretching surface subject to activation energy. *Journal of Thermal Analysis and Calorimetry, 148*(22), 12687-12697. [CrossRef]

[21] Ahmad, W. (2026). Three Dimensional Maxwell Tetra Hybrid Nanofluids Flow over a Riga Plate: Effect of Couple stress, Thermal Radiation, and Joule Heating. *Thermal Advances*, 100201. [CrossRef]

[22] Irfan, M., Khan, M., Muhammad, T., & Azeem Khan, W. (2025). Theory of activation energy and thermophoretic dispersion of nanoparticles in nonlinear radiative Maxwell nanofluid. *Waves in Random and Complex Media, 35*(2), 3996-4007. [CrossRef]

[23] Shahzad, F., Sagheer, M., & Hussain, S. (2019). MHD tangent hyperbolic nanofluid with chemical reaction, viscous dissipation and Joule heating effects. *AIP advances, 9*(2). [CrossRef]

[24] Qaiser, D., Zheng, Z., Riaz Khan, M., & Galal, A. M. (2026). Significance of activation energy and entropy optimization in radiative stagnation point flow of nanofluid with cross-diffusion and viscous dissipation. *Waves in Random and Complex Media, 35*(7), 14431-14452 .[CrossRef]

[25] Hussain, S., Haq, F., Ghazwani, H. A., Saleem, M., & Hussain, A. (2024). Entropy optimization in bio-convective chemically reactive flow of micropolar nanomaterial with activation energy and gyrotactic microorganisms. *Case Studies in Thermal Engineering, 55*, 104131. [CrossRef]

[26] Asjad, M. I., Sarwar, N., Ali, B., Hussain, S., Sitthiwirattham, T., & Reunsumrit, J. (2021). Impact of bioconvection and chemical reaction on MHD nanofluid flow due to exponential stretching sheet. *Symmetry, 13*(12), 2334. [CrossRef]

[27] Çolak, A. B. (2022). Analysis of the effect of Arrhenius activation energy and temperature dependent viscosity on non-Newtonian Maxwell nanofluid bio-convective flow with partial slip by artificial intelligence approach. *Chemical Thermodynamics and Thermal Analysis, 6*, 100039. [CrossRef]

[28] Ali, N. B., Mahmood, Z., Rafique, K., Khan, U., Adnan, Muhammad, T., & Kolsi, L. (2024). Exploring concentration-dependent transport properties on an unsteady Riga plate by incorporating thermal radiation with activation energy and gyrotactic microorganisms. *Applied Rheology, 34*(1), 20240019. [CrossRef]

[29] Khan, N. S., Shah, Z., Shutaywi, M., Kumam, P., & Thounthong, P. (2020). A comprehensive study to the assessment of Arrhenius activation energy and binary chemical reaction in swirling flow. *Scientific reports, 10*(1), 7868. [CrossRef]

[30] Irshad, S., Jahan, S., Sohail, M., & Ali, M. H. (2025). Exploring slip-enhanced MHD Williamson nanofluid dynamics: interplay of a permeable stretching sheet with thermal radiation and chemical reaction. *Pramana, 99*(1), 20. [CrossRef]

[31] Zeb, S., Gul, S., Shah, K., Santina, D., & Mlaiki, N. (2023). Melting heat transfer and thermal radiation effects on MHD tangent hyperbolic nanofluid flow with chemical reaction and activation energy. *Thermal Science, 27*(Spec. issue 1), 253-261. [CrossRef]

[32] Ahmad, W., Saqib, M., Khan, I., Oqilat, O., & Khan, M. S. (2025). Significance of Soret Dufour effects on MHD mixed convective flow of Maxwell hybrid nanofluid in porous medium with activation energy. *International Journal of Thermofluids, 28*, 101278. [CrossRef]

[33] Irfan, M. (2023). Energy transport phenomenon via Joule heating and aspects of Arrhenius activation energy in Maxwell nanofluid. *Waves in Random and Complex Media*, 1-16. [CrossRef]

[34] Jameel, M., Shah, Z., Rooman, M., Alshehri, M. H., Vrinceanu, N., & Antonescu, E. (2024). Entropy driven optimization of non-linear radiative chemically reactive sutterby nanofluid flow in presence of gyrotactic micro-organism with Hall effect and activation energy. *Scientific Reports, 14*(1), 30338. [CrossRef]

[35] Rashid, M., Alasiri, A., & Irfan, M. (2026). Entropy Generation Analysis on Magnetohydrodynamics (MHD) Blood Flow of Hybrid Nanofluid With Nonlinear Radiative Heat Flux. *ZAMM-Journal of Applied Mathematics and Mechanics/Zeitschrift für Angewandte Mathematik und Mechanik, 106*(7), e70508. [CrossRef]

[36] Alatawi, A., Alshaban, E., Aldhabani, M. S., & Alrihieli, H. (2025). Dynamic-behavior of Casson-type hybrid nanofluids due to a stretching sheet under the coupled impacts of boundary slip and reaction-diffusion processes. *Nanotechnology Reviews, 14*(1), 20250244.[CrossRef]

[37] Alsenafi, A., & Ferdows, M. (2021). Effects of thermal slip and chemical reaction on free convective nanofluid

from a horizontal plate embedded in a porous media. *Mathematical Biosciences and Engineering*, *18*, 4817-4833. [CrossRef]

[38] Prajapati, V. J., & Meher, R. (2024). Analysis of MHD tangent hyperbolic hybrid nanofluid flow with different base fluids over a porous stretched sheet. *Journal of Taibah University for Science*, *18*(1), 2300851. [CrossRef]

[39] Ahmad, W. (2026). Influence of Darcy-Forchheimer effects on 3D MHD rotating flow of casson hybrid nanofluid with velocity slip and convective boundary conditions. *ICCK Journal of Applied Mathematics*, *2*(1), 44-63. [CrossRef]

[40] Yusuf, A., Akolade, M. T., & Tijani, Y. O. (2024). Nonlinear mixed convective analysis of Thomson and Troian slip flow conditions for Ag-Cu-TiO_2/H_2O hybrid nanofluid over a Riga plate. *Journal of Computational and Theoretical Transport*, *53*(7), 553-574. [CrossRef]

[41] Revathi, G., Sajja, V. S., Babu, M. J., Srinivasa Babu, K. S., Suneel Kumar, A., Raju, C. S. K., & Yook, S. J. (2026). Multiple linear regression analysis on the flow of ternary hybrid nanofluid by a quadratically radiated stretching surface with and second order slip. *Waves in Random and Complex Media*, *36*(3), 3774-3791. [CrossRef]

[42] Bilal, S., & Yasir, M. (2025). Mass transpiration impact on effectiveness of heat transport of ternary hybrid nanofluid with velocity slip. *Case Studies in Thermal Engineering*, *73*, 106530. [CrossRef]

[43] Amer, A. M., Al Rashdi, S. A., Ghoneim, N. I., & Megahed, A. M. (2023). Tangent hyperbolic nanofluid flowing over a stretching sheet through a porous medium with the inclusion of magnetohydrodynamic and slip impact. *Results in Engineering*, *19*, 101370. [CrossRef]

[44] Sheri, S. R., Kallem, S. R., Perli, A. P., & Gollapalli, S. (2025). Magnetohydrodynamic flow of hyperbolic tangent fluid in a porous medium in the presence of slip, radiation and heat source effects. *Journal of Thermal Analysis and Calorimetry*, *150*(20), 16569-16584. [CrossRef]

[45] Shampine, L. F., Gladwell, I., Thompson, S., & Gladwell, I. (2003). *Solving ODEs with matlab* (Vol. 70). Cambridge: Cambridge university press. https://library.iigm.res.in/bib/6148

[46] Hale, N. (2006). A sixth-order extension to the MATLAB `bvp4c` software of J. Kierzenka and L. Shampine. *Department of Mathematics, Imperial College London*, 12-60. https://ora.ox.ac.uk/objects/uuid:8a565484-8be4-40a6-a5d3-b3d96d0e6859

[47] Ahmad, W. (2026). Significance of Riga plate on Marangoni convective flow of Casson hybrid nanofluid over a stretching/shrinking sheet with suction and Darcy-Forchheimer effects. *International Journal of Thermo-Fluid Systems and Sustainable Energy*, *2*(2), 30-50. [CrossRef]

[48] Ali, B., Jubair, S., Garayev, M., Khalifa, H. A. E. W., Kumar, A., & Shaaban, A. A. (2025). Energy and mass transfer through hybrid nanofluids flow comprised of AA7072-AA7075 nanoparticles subject to magnetic and thermal radiation on stretching surface. *Journal of Radiation Research and Applied Sciences*, *18*(1), 101250. [CrossRef]

Waqas Ahmad is with the Department of Physical and Numerical Sciences, Qurtuba University of Science and Information Technology, Peshawar, KP, Pakistan. His research interests include non-Newtonian and hybrid-nanofluid flow, magnetohydrodynamics, porous media, and computational heat and mass transfer. (Email: waqas64065@gmail.com)